Volume 18 | Number 1 | 7 January 2016 | Pages 1–636

PCCP

Physical Chemistry Chemical Physics
www.rsc.org/pccp

ISSN 1463-9076

ROYAL SOCIETY
OF CHEMISTRY

PERSPECTIVE
Darya Radziuk and Helmuth Möhwald
Ultrasonically treated liquid interfaces for progress in cleaning and separation processes

175 YEARS

ROYAL SOCIETY
OF CHEMISTRY

rsc.li/pccp

ARTICLE

Palladium–catalysed Alkyne Alkoxycarbonylation with P,N Chelating Ligands Revisited: A Density Functional Theory Study

Shahbaz Ahmad,[a] Ashley Lockett,[a] Timothy A. Shuttleworth[b] Alexandra Miles-Hobbs,[b] Paul G. Pringle[b] and Michael Bühl,*[a]

A revised *in situ* base mechanism of alkyne alkoxycarbonylation via a Pd catalyst with hemilabile P,N-ligands (PyPPh$_2$, Py = 2-pyridyl) has been fully characterised at the B3PW91-D3/PCM level of density functional theory. Key intermediates on this route are acryloyl (η^3-propen-1-oyl) complexes that readily undergo methanolysis. With two hemilabile P,N-ligands and one of them protonated, the overall computed barrier is 24.5 kcal mol^{-1}, which decreases to 20.3 kcal mol^{-1} upon protonation of the second P,N-ligand. This new mechanism is consistent with all of the experimental data relating to substituent effects on relative reaction rates and branched/linear selectivities, including new results on the methoxycarbonylation of phenylacetylene using (4-NMe$_2$Py)PPh$_2$ and (6-Cl-Py)PPh$_2$ ligand. This ligand is found to decrease catalytic activity over PyPPh$_2$, thus invalidating a formerly characterised *in situ* base mechanism.

[a.] School of Chemistry, University of St Andrews, North Haugh, St Andrews, Fife, KY16 9ST, UK, E-mail: buehl@st-andrews.ac.uk.
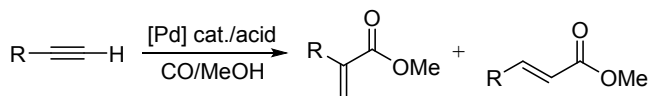[b.] University of Bristol, Cantocks Close, Bristol BS8 1TS, UK.
† Footnotes relating to the title and/or authors should appear here.
Electronic Supplementary Information (ESI) available: [details of any supplementary information available should be included here]. See DOI: 10.1039/x0xx00000x

Dedicated to Prof. Walter Thiel on the occasion of his 70th birthday

ARTICLE

Introduction

The regioselective, direct synthesis of fine chemicals from sustainable and abundant resources is highly desirable for industrial chemical manufacture. The key challenges within this area include the availability of commercially viable catalysts, efficient reaction time and conditions, realistic isolation procedures, broad substrate scope and high atom-economy. Using transition metal catalysts, homogeneously catalysed carbonylations are important industrial processes[1-5] that can be conducted with high chemo- and regioselectivities, efficiently extending carbon chains.[3,6] Transition metal catalysed alkoxycarbonylation (hydroesterification) of alkynes (Scheme 1) is a direct route to the corresponding acrylate esters with 100% atom economy.[7-14]
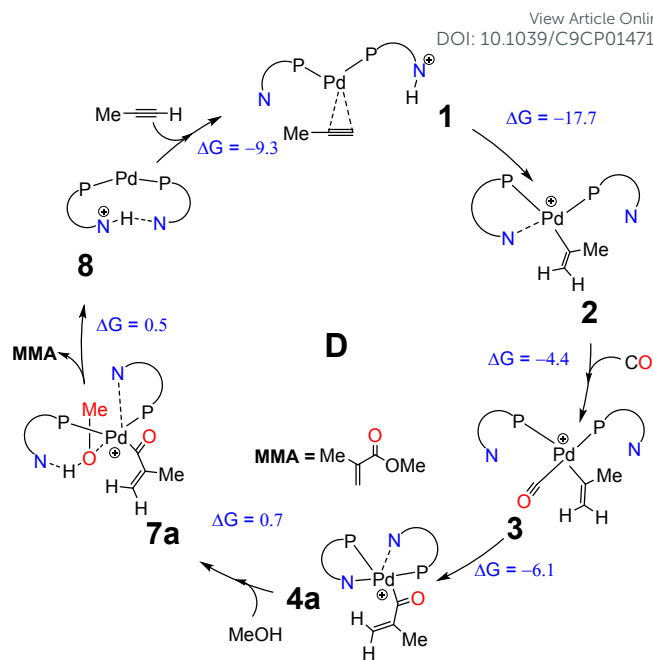
Scheme 1

Methoxycarbonylation of propyne yields methyl methacrylate (MMA),[7, 8, 15-21] the precursor to poly(methyl methacrylate), also known as Perspex.[22] There is a growing demand in the use of Perspex for liquid-crystal display (LCD) screens, especially in touch screen electronics.[23]

Currently, an important route to MMA on an industrial scale is a two-step process from ethene. The first step is the homogeneously catalysed methoxycarbonylation of ethene to yield methyl propionate (MeP) followed by a heterogeneously catalysed conversion of MeP to MMA.[22, 24-27]

Due to their hemilabile coordination modes, P,N-ligands are of considerable interest in homogeneous catalysis. Direct homogeneous methoxycarbonylation of propyne under mild conditions is an attractive route for the synthesis of MMA using a hemilabile Pd(P,N-chelate) catalyst.[7-10, 28-30] Drent's initial work suggested a carbomethoxy mechanism with termination involving intramolecular proton transfer from a protonated 2-pyridyl diphenylphosphine (PyPPh$_2$) ligand.[7] Subsequent labelling studies by Scrivanti *et al*. suggested that the cycle might be initiated by a proton transfer from PyPPh$_2$ onto coordinated alkyne.[7, 11]

The Bühl group has previously applied state-of-the-art density functional theory (DFT) studies to unravel the mechanistic details of homogeneous methoxycarbonylation of propyne using a hemilabile Pd(P,N-chelate) catalyst. A number of possible pathways (previously labelled **A - D**) were considered, of which only one appeared to be consistent with observed activities and selectivities (pathway **D**, Scheme 2).[29, 30] This mechanism involves proton shuttling by the pyridyl groups in the initiation and termination steps. The pendant pyridyl moiety (when protonated) can act as an *in situ* acid, protonating coordinated propyne followed by thermodynamically favoured CO insertion and then deprotonating coordinated methanol to promote rapid ester formation. The unfavourable steric interaction between the aromatic ring of the ligand and the methyl group of the propyne promotes the observed high regioselectivity (Scheme 2).

Scheme 2. Bühl's pathway **D,** including computed driving forces for elementary steps (ΔG^{298K} in kcal mol^{-1}).[29, 30]

Based on this mechanism, an increase in basicity of the 2-pyridyl moiety should facilitate the critical proton transfer steps, and indeed it was predicted computationally that the 4-dimethylamino-2-pyridyl ligand (4-Me$_2$N-Py)PPh$_2$ should lower the overall barrier of the whole cycle significantly, thus increasing the overall catalytic activity.[29] In the Pringle group we have put this prediction to the test for the methoxycarbonylation of phenylacetylene. Rather disappointingly, it transpires that the more basic ligand (4-Me$_2$N-Py)PPh$_2$ does not increase the activity over the parent PyPPh$_2$ and indeed, a decrease in activity is observed. We have thus revisited the original mechanism computationally and now present a new pathway that is consistent with all available experimental information.
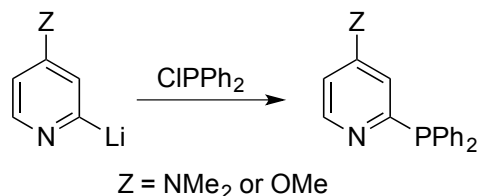
Results and Discussion

1. Methoxycarbonylation of Phenylacetylene

To test the predicted effect of the (4-Me$_2$N-Py)PPh$_2$ ligand, we synthesised it and used it in the Pd-catalysed methoxycarbonylation of phenylacetylene. We used this substrate rather than propyne, because it is a liquid at room temperature and thus more easily handled. We have confirmed computationally that our hypothesised mechanism is not dependent on this particular choice of substrate. We have recomputed pathway **D** at the same level, replacing the MeC≡CH with PhC≡CH. As documented in the Supporting Information (SI, see Table S1 and Figures S1 and S2) the general shape of the reaction profile, as well as key barriers are very similar on going from propyne to phenylacetylene. Importantly, for both substrates, essentially the same lowering in the overall barrier of the whole cycle is computed on going from the PyPPh$_2$ to the (4-Me$_2$N-Py)PPh$_2$ ligand (see SI). Predictions made for propyne as substrate should thus be entirely transferable to phenylacetylene.

We had anticipated that the dimethylamino group in (4-Me$_2$N-Py)PPh$_2$ would be sufficiently basic to be protonated in the very

acidic conditions under which the catalysis is carried out and therefore may not produce the desired electron-rich pyridyl group. For this reason, in addition to the previously reported (4-Me$_2$N-Py)PPh$_2$ we also prepared the p-anisyl ligand (4-MeO-Py)PPh$_2$ by a similar route (Scheme 3) in the belief that this would have the properties of an electron-rich pyridyl substituent without a significant risk of protonation of the methoxy substituent.

Scheme 3. Preparation of (4-Me$_2$N-Py)PPh$_2$ and (4-MeO-Py)PPh$_2$

The phenylacetylene methoxycarbonylation (Scheme 1, R = Ph) results obtained under the standard conditions (Method A in the Experimental) with the 2-pyridylphosphines are given in Table 1. It is clear that the catalysts derived from (4-Me$_2$N-Py)PPh$_2$ and (4-MeO-Py)PPh$_2$ are not as active as the parent PyPPh$_2$.

Table 1 Catalytic methoxycarbonylation of phenylacetylene.

Entry	Ligand[a]	M [b]	Conv at 15 min[b]	Conv at 1 h[c]	Conv at 4.5 h[c]	Selectivity[d]
1	PyPPh$_2$	A		99	100	99
2	(4-Me$_2$N-Py)PPh$_2$	A		51	78	95
3	4-MeO-Py)PPh$_2$	A		86	98	99
4	PyPPh$_2$	B	88			>99
5	(6-Cl-Py)PPh$_2$	B	99			>99

[a] Py = 2-pyridyl. [b]Reaction conditions are given in the Experimental Section. Method A was used for Entries 1-3 and Method B for Entries 4-5. [c]Conversion and selectivity determined by ^{1}H NMR. Each result is an average of 2 or more runs. [cd]The rest of the product was the linear isomer.
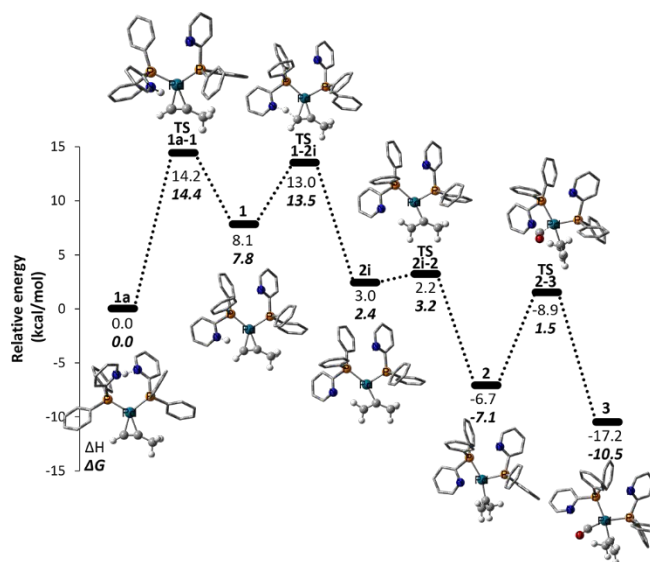
Since these new results do not support our previously proposed mechanism, pathway **D**, we have revisited the mechanism computationally and have uncovered a new pathway which is consistent with the experimental results. For consistency with our previous results we will label the new pathway **E**.

2. Revised *In Situ* Base Mechanism (E)

2.1 General Mechanism. A more detailed conformational analysis of the PyPPh$_2$ ligands in intermediates **1** - **9** has now revealed that some rotamers with different orientation of the Py substituent are slightly lower in energy than the ones reported previously. In addition, we have located the transition states of all steps that involve addition of reactants or dissociation of product, which had been neglected before. None of these refinements resulted in any qualitative changes of the mechanism. Such a qualitative change was found, however, when the acyl intermediate (**4a** in Scheme 2) was scrutinised further. What has been revealed is that an isomeric acryloyl complex is accessible (complex **4** discussed below), which is slightly higher in energy than **4a** by 1.1 kcal mol^{-1}. On pathway **D**, migratory CO insertion into **4a** afforded a loosely bound MMA product that was easy to dissociate from the metal.

In contrast, migratory insertion in the new complex **4** affords a very stable product complex with strongly bound MMA (complex **7** discussed below). This new thermodynamic sink on pathway **D**, which had been overlooked before, would raise the overall free-energy span of the whole cycle from 22.9 kcal mol^{-1} [29, 30] to 41.5 kcal mol^{-1} (adding the free-energy difference between the present isomer **7** and the previous **TS5–6**), which would seem to be difficult to overcome even at the elevated experimental temperature. However, a new mechanism for methanolysis of the acryloyl complex was found with a significantly lower barrier than that of the acyl complex (**7a** in Scheme 2), which makes the whole process viable again. Based on these findings we have now traced a complete cycle (termed pathway **E**), which is discussed in detail below.
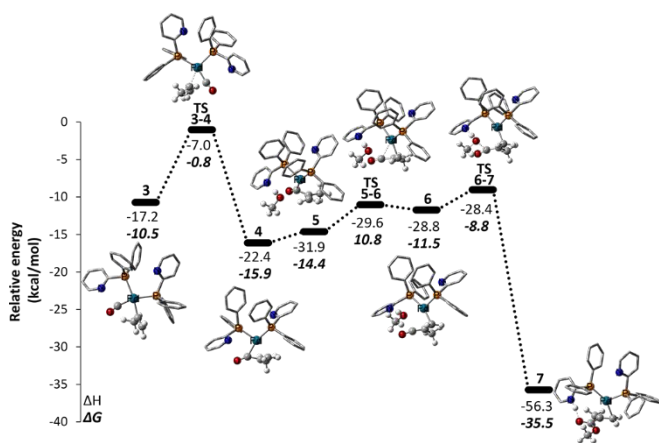
In addition, another isomer of complex **1** has been located, which is stabilised through an intramolecular NH···N hydrogen bond (**1a**, Figure 1), and which is now taken as the zero point of all our energies. Before initiating the whole reaction by protonating the coordinated alkyne, **1a** first must rearrange to Pd(II) complex **1** ($\Delta G_{1a\rightarrow1}$ = 7.8 kcal mol^{-1} and $\Delta G^{\ddagger}_{1a\rightarrow1}$ = 14.4 kcal mol^{-1}). The protonation of propyne in complex **1** gives rise to an agostic intermediate **2i** ($\Delta G_{1\rightarrow2i}$ = -5.4 kcal mol^{-1} and $\Delta G^{\ddagger}_{1\rightarrow2i}$ = 5.7 kcal mol^{-1}). A low kinetic barrier via **TS2i–2** suggests a fast conversion of **2i** into **2** ($\Delta G_{2i\rightarrow2}$ = -9.5 kcal mol^{-1} and $\Delta G^{\ddagger}_{2i\rightarrow2}$ = 0.8 kcal mol^{-1}). CO displaces the chelating nitrogen of the pyridyl moiety via **TS2–3** forming intermediate **3** ($\Delta G_{2\rightarrow3}$ = -3.4 kcal mol^{-1} and $\Delta G^{\ddagger}_{2\rightarrow3}$ = 8.6 kcal mol^{-1}) through a large enthalpic gain (Figure 1). This part is essentially identical to the previous pathway **D**, except for some minor modifications of the energetics from the differences in conformations.

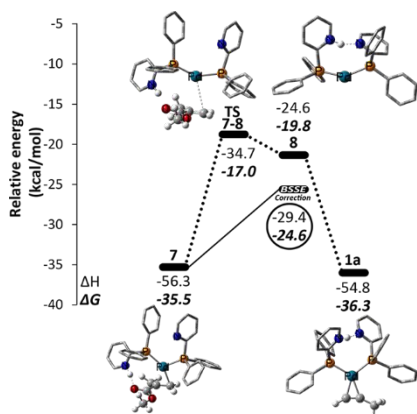**Figure 1.** Free energy profile using methanol as the model solvent for initial proton transfer and CO uptake (B3PW91-D3/ECP2/PCM level). Energies (ΔH and ΔG) are in kcal mol^{-1} relative to **1a**.

The key step is now the direct formation of the acyloyl complex **4** through migratory CO insertion (Figure 2, the electronic structure of this complex is discussed below). The final step of methanolysis

has now been divided into two sub-steps, the one that leads to the production of MMA and the other that dissociates MMA from the catalytic system (Figure 2 and Figure 3, respectively). In the first sub-step, MeOH associates to the complex via a hydrogen bonding MeO–H.....N interaction to the nitrogen of one of the 2-PyPPh$_2$ moieties giving rise to an intermediate **5** ($\Delta G_{4\rightarrow5}$ = 1.5 kcal mol^{-1}). Then, the acryloyl group rearranges via **TS5–6** ($\Delta G_{5\rightarrow6}$ = 2.9 kcal mol^{-1} and $\Delta G^{\ddagger}_{5\rightarrow6}$ = 3.6 kcal mol^{-1}) to form a very reactive ketene-like intermediate. The associated MeOH can easily perform a nucleophilic attack at the activated acyl group of the ketene via **TS6 –7**, assisted by the nearby Py group which acts as an *in situ* base accepting the proton from MeOH (Figure 4). This step leads to the formation of a low-lying MMA coordinated product **7** ($\Delta G_{6\rightarrow7}$ = -24.1 kcal mol^{-1} and $\Delta G^{\ddagger}_{6\rightarrow7}$ = 2.7 kcal mol^{-1}). The ease of this step with its very low barrier is remarkable if one recalls that on pathway **D**, methanolysis of the acyl complex **7a** is the most difficult step, with the highest activation energy.
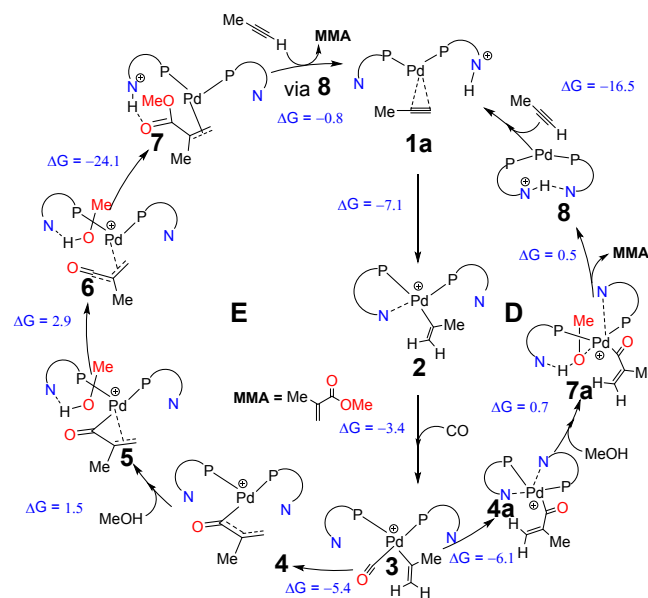

Figure 2. Carbonylation, MeOH uptake, and formation of ketene and MMA. Energies are (ΔH and ΔG) in kcal mol^{-1} relative to **1a**.

Figure 3. MMA dissociation and regeneration of **1a**. Energies are in kcal mol^{-1} relative to **1a**. The solid line indicates free energies corrected for basis-set superposition error (BSSE), with the BSSE-corrected ΔH and ΔG encircled.

In **7**, MMA is strongly bound to the metal atom and full dissociation is highly endergonic, with a computed ΔG of 11.0 kcal mol^{-1} (for the reaction **7** $\rightarrow$ [Pd(PyPPh$_2$)(HPyPPh$_2$)]$^+$ (**8**) + MMA). We located a number of associative interchange pathways where

MMA is replaced with fresh reactant, propyne, through transition states with four ligands coordinated to Pd. However, the full MMA dissociation indicated to be more favourable than all the other pathways (with a kinetic barrier of $\Delta G^{\ddagger}_{7\rightarrow8}$ = 16.8 kcal mol^{-1}). The propyne uptake to **8** regenerates the complex **1a** ($\Delta G_{8\rightarrow1a}$ = -16.5 kcal mol^{-1}).

Scheme 4. Catalytic cycle of pathways **D** (right) and **E** (left) involving P,N ligand as an *in Situ* Base, according to DFT, including computed driving forces for elementary steps (ΔG^{298K} in kcal mol^{-1}).

The key intermediates in pathway **E** are the acryloyl complexes **4 - 6**. Such complexes are known (for selected examples see references 31-36), but their involvement in alkoxycarbonylation has, to our knowledge, not been suggested before. From the optimised structures in Figure 4 and the bond distances in Table 2 it can be seen how, upon addition and reorientation of MeOH, the metal atom is displaced from a position closer to the carbonyl C atom to the terminal methylene group. In isomer **6** the ligand has significant ketene character, apparent from the short C2-C3 distance and an increased C2-C3-Oa bond angle approaching 180°. The trends in bond distances are reflected in the computed Wiberg bond indices (WBIs), a measure for the covalent character of a bond[37] (which tends to adopt values close to 1 and 2 for covalent single and double bonds, respectively, affording lower values for bonds with high ionic character such as the Pd-C bonds in Table 2).
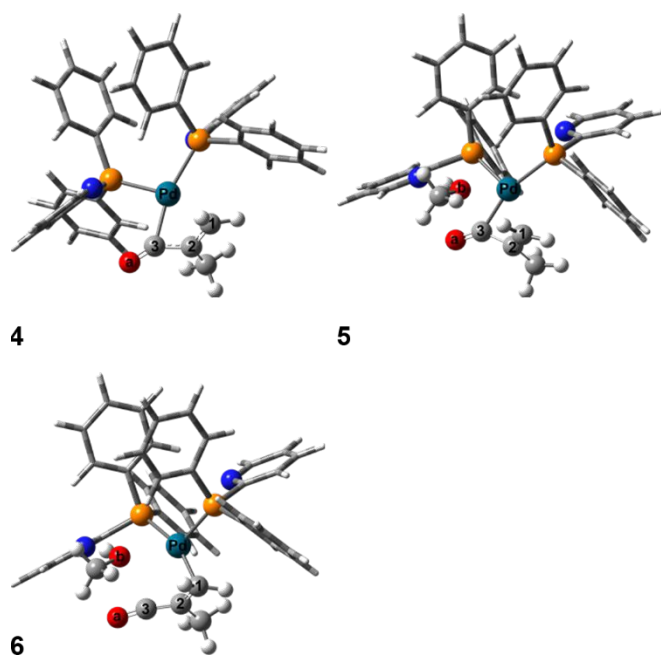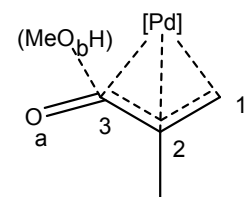
Figure 4. Optimised structures of intermediates 4-**6**

Scheme 5. Labelling scheme for complexes **4** - **6**.

Table 2: Selected bond distances (in Å) with Wiberg bond indices [in square brackets] of complexes **4 - 6**, as well as selected bond angles (in degrees, for atom labelling see Scheme 5), B3PW91-D3/ECP2/PCM level.

Parameter	4	5	6
d(Pd-C1)	2.213 [0.38]	2.295 [0.31]	2.063 [0.53]
d(Pd-C2)	2.236 [0.20]	2.263 [0.18]	2.265 [0.20]
d(Pd-C3)	2.104 [0.48]	2.054 [0.54]	2.757 [0.15]
d(C1-C2)	1.398 [1.46]	1.382 [1.56]	1.446 [1.20]
d(C2-C3)	1.435 [1.18]	1.457 [1.11]	1.361 [1.40]
d(C3-Oa)	1.183 [1.95]	1.187 [1.93]	1.159 [2.08]
d(C3-Ob)	n.a.	3.481 [0.00]	2.966 [0.02]
a(C1-C2-C3)	114.8	114.8	120.3
a(C2-C3-Oa)	146.1	140.8	170.8

In the pathways discussed so far, we have assumed that only one of the PyPPh$_2$ ligands is protonated. Under the strongly acidic conditions, however, it may well be possible that a significant fraction of the catalyst has both ligands protonated. We have therefore recalculated the crucial steps on pathways **E** for diprotonated, dicationic intermediates (see Figure S3 in the SI). Introduction of the second proton decreases the MMA dissociation barrier to 13.2 kcal mol^{-1}, but the overall barrier remains comparable to that of monocationic pathway, as now the overall barrier has been shifted to the proton transfer step rather than the product dissociation step (**7$^+$** + Propyne → **TS1–2i$^+$** + MMA, ΔG‡ = 16.8 kcal mol^{-1}). The concomitant quantitative

changes to the energetics along with the selectivity and substituent effects are discussed below.
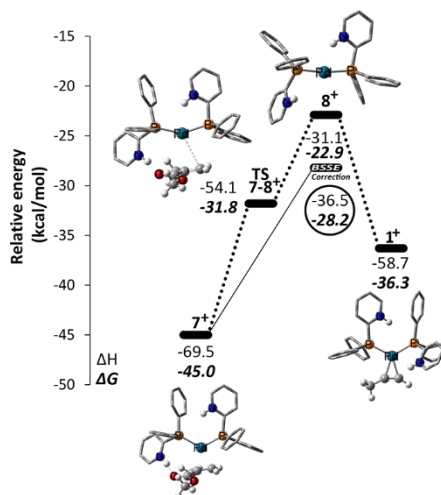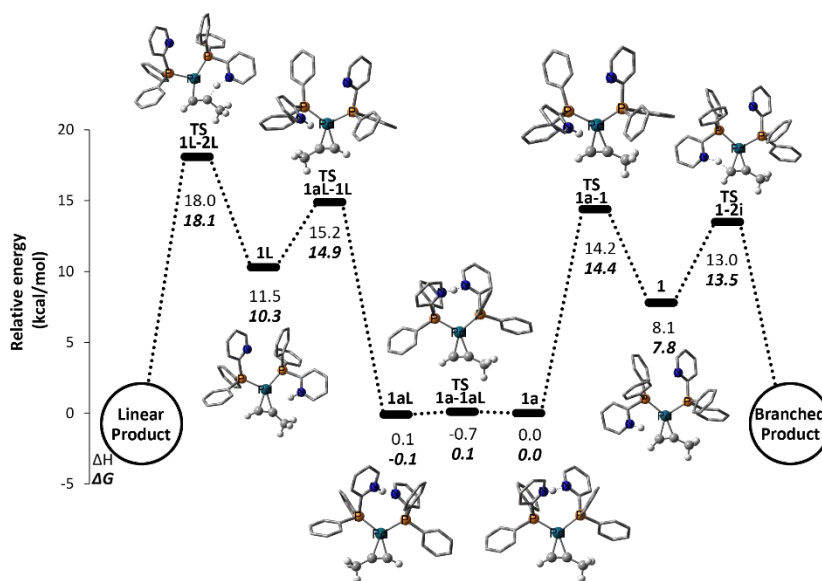

Figure 5 Intermediates for product release on the dicationic version of pathway **E**. The solid line indicates BSSE-corrected free energies, with BSSE-corrected ΔH and ΔG encircled.

2.2 Selectivity and substituent effects. The pathways discussed so far produce branched MMA, the main product observed experimentally. The linear/branched selectivity is determined early on the path, upon intramolecular protonation of coordinated propyne in **1**. This step in our new pathway **E** is the same as in the original pathway **D** (where observed selectivities are well reproduced). The minor changes in conformational preferences found in the present work lead to negligible changes in the final energetics: Intermediate **1** (leading to a branched product) is more stable by ΔG = 2.5 kcal mol^{-1} (ΔH = 3.4 kcal mol^{-1}) than intermediate **1L** (leading to the linear product). The appearance of the new intermediate **1a** and its equivalent **1aL** (leading to the linear product) slightly affects the computed selectivities, because the highest point on the branched pathway is **TS1a-1** (i.e. formation of **1**), whereas on the linear pathway it is **TS1-2L** (i.e. the protonation of the alkyne, see Figure 6). The two kinetic barriers leading to the isomeric products differ by ΔΔG‡ = 3.7 kcal mol^{-1}, corresponding to a high selectivity towards the branched product at 45 °C (Table 3), which is consistent with the experimental results. On the dicationic pathway, no isomer corresponding to **1a** exists, and the selectivity is determined by the difference between **TS1-2i$^+$** and **TS1L-2L$^+$** (see Figure S4), affording a slightly reduced ΔΔG‡ = 2.9 kcal mol^{-1}.

Substituting the Py moiety with a 6-Me-Py group further enhances the selectivity toward the branched product. This is fully borne out in our calculations, where the greater steric effects on going from PyPPh$_2$ to by (6-Me-Py)PPh$_2$ increases ΔΔG‡ from 3.7 kcal mol^{-1} to 6.3 kcal mol^{-1}. The latter value corresponds to a selectivity of 99.99%, in good agreement with the experimental observations towards selectivity.

Figure 6. Pathways for formation of branched (right) and linear (left) products; energies (*ΔH* and *ΔG*) are in kcal mol^{-1} relative to **1a**. Selectivity is governed by the difference between **TS1a-1** and **TS1-2L.**

ARTICLE

In the context of the overall activities discussed in the next section, we also evaluated the selectivity-determining difference in the free energy barrier for two other ligands with NMe_2 and Cl substituents in 4- and 6-positions of the 2-pyridyl moiety, respectively. In all these cases, the high branched selectivity is predicted to be maintained or slightly enhanced ($\Delta\Delta G^{\ddagger}$ values in upper half of Table 3). Only for the dicationic mechanism with $PyPPh_2$ and (4-Me_2N-Py)PPh_2 ligands, a slight reduction in selectivity would be predicted (lower half of Table 3).

Table 3: Effects of different 2-pyridylphosphine ligand systems on branched to linear products selectivities[*a*] and the overall energy barriers (energy span, $\Delta G^{\ddagger}_{MARI \to HETS}$). All the values are given in kcal mol^{-1}.

Ligand	$\Delta\Delta G^{\ddagger}$	% Branched (at 45 °C)	Energy Span
Mechanism E			
$PyPPh_2$	3.7	99.71	16.8
(6-Me-Py)PPh_2	6.3	99.99	16.8
(4-Me_2N)$PyPPh_2$	4.4	99.91	18.2
(6-Cl-Py)PPh_2	5.9	99.99	15.9
(4-Cl-Py)PPh_2	4.8	99.95	17.9
Mechanism E			
(Dicationic)			
$PyPPh_2$	2.9	98.99	16.8
(6-Me-Py)PPh_2	4.7	99.94	18.2
(4-Me_2N-Py)PPh_2	2.5	98.12	19.6
(6-Cl-Py)PPh_2	5.7	99.99	16.4
(4-Cl-Py)PPh_2	3.8	99.78	16.7

[*a*]For mechanism E, $\Delta\Delta G^{\ddagger} = \Delta G^{\ddagger}_{1L \to 2L} - \Delta G^{\ddagger}_{1 \to 1a}$ (cf. Table S6), for mechanism E (dicationic), $\Delta\Delta G^{\ddagger} = \Delta G^{\ddagger}_{1L \to 2L^+} - \Delta G^{\ddagger}_{1 \to 2i^+}$ (cf. Figure S4)

2.3 Catalytic activity and substituent effects. The overall kinetic efficiency and, in particular, substituent effects on it, can be evaluated using Kozuch and Shaik's[38-40] energetic span model. This model identifies the rate-limiting states (as opposed to a single rate-limiting step) as those that maximise the energy difference between the lowest intermediate and the highest transition state on a continuous (free-)energy profile of a catalytic cycle. On the monocationic reaction pathway **E**, we have identified intermediate **7** as the most abundant reaction intermediate (MARI) and **TS7–8** as highest energy transition state (HETS). The resulting overall barrier between MARI and HETS is 16.8 kcal mol^{-1}, consistent with a high TOF at 45 °C. For pathway **D**, the overall barrier was originally reported to be 22.9 kcal mol^{-1}, however this value is erroneous because one of the important intermediates, namely **7** in the current investigation (which is the MARI for pathway **E**) was overlooked and missing from the reaction profile. The MARI on the reaction profile of pathway **E** is more stable by 19.3 kcal mol^{-1} in free energy (21.6 kcal mol^{-1} in enthalpy) than the MARI on the reaction profile of pathway **D**. Thus, the original pathway **D** with its

HETS for methanolyis of the acyl complex should have an actual overall free energy barrier of more than 40 kcal mol^{-1}, much too high to be overcome under the experimental conditions.

For the original pathway **D**, introduction of an NMe_2 group in 4-position of the 2-Py moiety was predicted to lower the overall barrier notably (by 3.6 kcal mol^{-1}).[29, 30] In contrast, in our new mechanism **E**, the same substitution raises the overall barrier from 16.8 kcal mol^{-1} to 18.2 kcal mol^{-1} (see energy span values in upper half of Table 3). This increase in the overall barrier should decrease the TOF relative to that of the original system, in good agreement with the experimental results discussed in Section 1. The reason for this different substituent effect in pathways **D** and **E** is that in the former, the highest transition state (HETS) is that for methanolysis, which is significantly reduced as the basicity of the Py group is increased, whereas in the latter (pathway **E**), the HETS is for product release, which is only little affected by the basicity of the ligand.

For the dicationic route, which we would expect to become more relevant with decreasing pH, an overall barrier of 16.8 kcal mol^{-1} between MARI and HETS is computed, i.e. same as that on the monocationic pathway **E**. The MARI on both pathways (monocationic and dicationic) are **7** and **7$^+$**, though different species were identified controlling the overall turnover frequency (X_{TOF}). Details of X_{TOF} for the dicationic pathway are given in Table S4. Going from the $PyPPh_2$ to the (4-Me_2N-Py)PPh_2 ligand on the dicationic pathway slightly increases the overall barrier, from 18.2 kcal mol^{-1} to 19.6 kcal mol^{-1} (which should decrease the predicted TOF).[41]

Since an increase of ligand basicity causes the overall activity to decrease slightly, a reduction of basicity might actually have the opposite effect, i.e. increase the overall activity. In order to test this possibility computationally, we considered two chlorinated derivatives. When a Cl atom is placed on the 4-position of the pyridyl moiety, an increase in the overall free energy span is predicted on the monocationic pathway; however the overall free energy span slightly decreased for the dicationic pathway (Table 3). When the Cl atom is placed on the 6-position (thereby combining electronic and steric effects), a slight decrease in the overall barrier is predicted for both monocationic and dicationic pathways (by 0.9 kcal mol^{-1} and 0.5 kcal mol^{-1}, compare entries for $PyPPh_2$ and (6-Cl-Py)PPh_2 in Table 3).[41] At low pH, our calculations suggest that this ligand would thus impart an increase in activity. Encouragingly, this prediction is supported by the results obtained at Shell[42] which show a significant increase in activity with the (6-Cl-Py)PPh_2 ligand, in the methoxycarbonylation of propyne albeit under slightly different reaction conditions [reaction temperature 30°C and 45°C for $PyPPh_2$ and (6-Cl-Py)PPh_2, respectively]. We have also tested the activity of the catalyst derived from (6-Cl-Py)PPh_2 in the methoxycarbonylation of phenylacetylene and found that the (6-Cl-

Physical Chemistry Chemical Physics Accepted Manuscript

Py)PPh$_2$ ligand does indeed produce a more active catalyst under the same conditions (Table 1, Entries 4 and 5) as predicted.

Conclusions

In summary, we have tested predictions based on DFT about how to increase the activity of palladium catalysts with P,N hemilabile ligands in alkyne alkoxycarbonylation. The simple ligand substitution from in silico design, namely going from PyPPh$_2$ to the (4-Me$_2$-N)PyPPh$_2$ ligand, was realised experimentally, but failed to produce the predicted rate enhancement. We have thus revisited and revised the originally proposed mechanism (**D**) computationally at the B3PW91-D3/PCM level of density functional theory. On reaction profiles of the revised mechanism (**E**), highly reactive acryloyl and ketene-type intermediates are identified, which have very low barriers for the alcoholysis step and an overall kinetic barrier of $\Delta G^{\ddagger}$ = 16.8 kcal mol^{-1}.

Barriers controlling branched/linear selectivity are comparable in both pathways **D** and **E**, which are improved on going from 2-PyPPh$_2$ to (6-Me-Py)PPh$_2$ and (6-Cl-Py)PPh$_2$ ligand systems towards the branched-forming route. Both (6-Me-Py)PPh$_2$ and (6-Cl-Py)PPh$_2$ ligand systems are analogous to each other on controlling the selectivities, and the latter also decreases the overall barrier to 15.9 kcal mol^{-1}.

Under higher acid concentrations, modeled by two protonated P,N-ligands, alkyne alkoxycarbonylation may follow the dicationic version of *in situ* base mechanism, again with an overall barrier of 16.8 kcal mol^{-1}

Unlike the results obtained for the original pathway **D**, on the new pathway **E** the (4-Me$_2$N-Py)PPh$_2$ ligand system is now indicated to decrease the catalytic activity. On the other hand, a slight decrease in the overall barrier is predicted for the (6-Cl-Py)PPh$_2$ ligand system at higher acid concentrations. This prediction was tested experimentally and the results show that the (6-Cl-Py)PPh$_2$ does indeed produce a more active catalyst for the carbonylation of phenylacetylene.

We hope that our detailed computational insights will help in the design of further improved catalysts for carbonylation by tuning the stereoelectronic properties of the ligand.

Experimental Section

Ligand Synthesis and Catalysis

All reactions were carried out under an atmosphere of dry nitrogen, unless otherwise stated, using standard Schlenk line techniques and oven dried (200 °C) glassware. CH$_2$Cl$_2$, Et$_2$O, THF, toluene and hexane were collected from a Grubbs type solvent purification system,[43] and deoxygenated by bubbling with N$_2$ for 30 minutes. CD$_2$Cl$_2$ was dried over activated 4 Å molecular sieves for 72 hours and deoxygenated by successive freeze-pump-thaw cycles. MeOH was purchased as anhydrous, stored over 3 Å molecular sieves and deoxygenated by bubbling with N$_2$ for 30 minutes. ^{1}H, ^{13}C and ^{31}P and NMR spectra were recorded at ambient temperature unless otherwise stated on Jeol ECP (Eclipse) 300, Jeol ECS 300, Jeol ECS 400, Varian 400-MR, Varian VNMRS 500 spectrometers and a Bruker Avance III HD 500 spectrometer equipped with a ^{13}C-observe

(DCH) cryogenic probe. Chemical shifts δ are given in parts per million (ppm) and coupling constants J are in Hz. ^{1}H and ^{13}C chemical shifts were referenced to residual solvent peaks. ^{31}P chemical shifts were referenced to 85% H$_3$PO$_4$. Mass Spectra were recorded by the University of Bristol Mass Spectrometry Service on a VG Analytical Autospec (EI) or VG Analytical Quattro (ESI) spectrometer. Elemental Analysis was carried out by the Microanalytical Laboratory of the School of Chemistry, University of Bristol. Thin Layer Chromatography (TLC) was performed using Merck Kieselgel 60 F254 (Merck) aluminium backed plates (0.25 mm layer of silica). Flash column chromatography was performed using a Biotage Isolera Spektra One Chromatographic Isolation system and the solvent system stated. DMAE (dried over 4 Å molecular sieves) was purchased from commercial suppliers and purified before use. Other commercial reagents were used as supplied unless otherwise stated. PyPPh$_2$,[44] (4-Me$_2$N-Py)PPh$_2$[45] were made by literature procedures.

Synthesis of (4-OMe-Py)PPh$_2$

2-Bromo-4-methoxypyridine (0.500 g, 2.66 mmol) was dissolved in Et$_2$O (10 cm^3). This was cooled to -78 °C and n-BuLi (1.70 cm^3, 2.72 mmol, 1.6 M in hexanes) was added dropwise, giving a bright orange solution. After stirring for 30 minutes at this temperature, ClPPh$_2$ (0.40 cm^3, 2.22 mmol) was added dropwise and the reaction allowed to warm to ambient temperature and was stirred for 2 hours, after which deoxygenated H$_2$O (10 cm^3) was added to quench the reaction. The Et$_2$O layer was extracted and the aqueous layer washed with Et$_2$O (2 x 10 cm^3). The organic portions were collected, dried over Na$_2$SO$_4$, filtered and the solvent removed *in vacuo* to yield the crude mixture as a pink oil. Recrystallisation from hexane (*ca.* 5 cm^3) at -20 °C gave the product as an off white solid (0.527g, 81%). ^{1}H NMR (400 MHz, CD$_2$Cl$_2$): δ_H 8.50-8.49 (m, 1H, py$H$ (H-6)), 7.42-7.33 (m, 10H, ph$H$), 6.73-6.71 (m, 1H, py$H$ (H-5)), 6.66-6.65 (m, 1H, py$H$ (H-3)), 3.72 (s, 3H, OCH_3). ^{13}C{^{1}H} NMR (126 MHz, CD$_2$Cl$_2$): δ_C 166.1 (d, $^1J_{C,P}$ = 4.5 Hz, py$C$ (C-2)), 165.6 (d, $^3J_{C,P}$ = 4.2 Hz, py$C$ (C-4)), 152.0 (d, $^3J_{C,P}$ = 13.5 Hz, py$C$ (C-6)), 137.0 (d, $^1J_{C,P}$ = 10.8 Hz, ph$C$ (C-1)), 134.7 (d, $^2J_{C,P}$ = 19.9 Hz, ph$C$ (C-2 and C-6)), 129.6 (s, ph$C$ (C-4)) , 129.1 (d, $^3J_{C,P}$ = 7.2 Hz, ph$C$ (C-3 and C-5)), 115.3 (d, $^2J_{C,P}$ = 20.1 Hz, py$C$ (C-3)), 108.4 (s, py$C$ (C-5)), 55.6 (s, OCH_3). ^{31}P{^{1}H} NMR (162 MHz, CD$_2$Cl$_2$): δ_P -2.8 (s, Ph$_2$PR). HR-MS (EI): *m/z* calc. for C$_{18}$H$_{16}$NOP [M]$^+$ = 293.0970; obs. = 293.0980. Elem. Anal. found (calc. for C$_{18}$H$_{16}$NOP): C, 73.26 (73.61); H, 5.30 (5.50); N, 4.76 (4.73).

Synthesis of (6-Cl-Py)PPh$_2$

This ligand was made by a modification of a literature method.[46] Ph$_2$PH (2.52 g, 13.5 mmol) in THF (15 cm^3) was cooled to -78 °C and n-BuLi (8.45 cm^3, 13.5 mmol, 1.6 M in hexanes) was added dropwise, giving a bright orange solution. After stirring the reaction mixture for 30 min at -78 °C, the reaction allowed to warm to ambient temperature and was stirred for 1 hour. The reaction mixture was then added dropwise to a solution of 2,6-Dichloropyridine (2.00 g, 13.5 mmol) in THF (20 cm^3) at -78 °C. The reaction allowed to warm to ambient temperature and was stirred for 18 hours. Volatiles were removed *in vacuo* and the reaction was dissolved in toluene (20 cm^3). Deoxygenated H$_2$O (20 cm^3) was then added. The toluene layer was extracted and the aqueous layer washed with toluene (3 x 10 cm^3). The organic portions were collected, dried over MgSO$_4$, filtered and the solvent removed *in vacuo* to yield the crude mixture as a pale orange solid. Recrystallisation from MeOH gave the product as a white solid (2.44 g). The MeOH supernatant was then placed in a -20 °C freezer where precipitation occurred. The supernatant was removed and

Journal Name

ARTICLE

any remaining solvent removed *in vacuo* to yield additional product as a white solid (combined yield = 2.97 g, 74%). ^{31}P, ^{13}C and ^{1}H NMR data all agreed with the literature values.[47]

Catalytic methoxycarbonylation of phenylacetylene

Adapted from previously reported procedure.[48] Catalysis was performed using a Baskerville "Multi-Cell" autoclave.

Method A: The ligand (0.110 mmol) was added to the autoclave and the system put under an atmosphere of N_2. Solutions of $Pd(OAc)_2$ (5.50 x 10^{-3} mmol) in MeOH (0.5 cm^3) and $TsOH.H_2O$ (0.220 mmol) in MeOH (0.5 cm^3) were added, followed by phenylacetylene (5.50 mmol). This was then washed in using MeOH (0.5 cm^3) and the autoclave flushed with three cycles of CO (*ca.* 10 bar). The autoclave was then pressured to 45 bar and heated to 60 °C. After either 1 hour or 4.5 hours, the autoclave transferred to an ice bath and once cooled, the system was vented.

Method B: The ligand (0.55 x 10^{-3} mmol) was added to the autoclave and the system was put under an atmosphere of N_2. Solutions of $Pd(OAc)_2$ (2.75 x 10^{-3} mmol) in MeOH (0.5 cm^3) and $TsOH.H_2O$ (0.10 mmol) in MeOH (0.5 cm^3) were added, followed by phenylacetylene (5.50 mmol). This was then washed in using MeOH (0.5 cm^3) and the autoclave was flushed with three cycles of CO (*ca.* 10 bar). The autoclave was then pressurised to 45 bar and heated to 60 °C. After 15 minutes, the autoclave was transferred to an ice bath and once cooled, the system was vented.

For both methods A and B, a small sample of the product was dissolved in $CDCl_3$ and analysed by ^1H NMR spectroscopy. Conversion and selectivity was determined by integration of the phenylacetylene alkynyl proton (δ_H 3.10 ppm) and the methyl atropate (δ_H 6.38 and 5.90 ppm) and methyl cinnamate (δ_H 7.71 and 6.42 ppm) alkenyl protons (see SI for the spectra).

DFT Computations

We have used B3PW91[49-51] hybrid functional, which has been successfully validated to study related (2-pyridyl)thiourea Pd(II) complexes[52] and for a range of reactions that rely upon metals.[53-56] When coupled with Grimme's DFT-D3,[57-59] including Becke-Johnson damping,[60, 61] this functional benchmarks well against explicitly correlated CCSD(T).[62] DFT-D3BJ correction has been computed for the minimised geometries.

Geometries of all complexes were fully optimized at the B3PW91/ECP1 level, where ECP1 corresponds with the 6-31G** basis set on all nonmetal atoms, in conjunction with the SDD basis on Pd, denoting the small-core Stuttgart-Dresden relativistic effective core potential (ECP) together with its valence basis set. The nature of all the possible minima and transition states was verified by frequency calculations within the harmonic approximation. Harmonic frequencies were computed analytically and were used to obtain enthalpic corrections from standard thermodynamic expressions at 298.15 K. Thermochemical correction terms δE_G were carried out as difference of the reaction free energy of a given step ($\Delta E_{B3PW91/ECP1}$) and the corresponding free energy ($\Delta G_{B3PW91/ECP1}$):

$$\delta E_G = \Delta G_{B3PW91/ECP1} - \Delta E_{B3PW91/ECP1} \qquad (1)$$

To obtain starting structures for the transition states, connecting the intermediates, potential energy profile calculations were performed at the same level, B3PW91/ECP1. All potential energy profile calculations were computed by increasing the metal–ligand distance by 0.1 Å and optimizing the remaining geometric parameters using loose convergence criteria. Taking the highest points of these paths, full transition state optimisations were performed using QST3 algorithm[63] and were confirmed to link to

the respective reactants and products using intrinsic reaction coordinate (IRC) calculations.[64, 65]

The energies of the pre-optimised complexes were refined using the same functional and an ECP2 level. At this level Pd was treated with the same SDD pseudopotential and valence basis as in ECP1 whereas 6-311+G** basis set was used for all other atoms. Solvent effects were included by a polarisable continuum (PCM)[66-68] model with methanol as a solvent. DFT-D3BJ corrections were added to accurately account for the missing dispersion. The final ΔG and ΔH values are calculated as:

$$\Delta G = \Delta E + \delta E_{Solv} + \delta E_{DFTD3BJ} + \delta E_G \qquad (2)$$

$$\Delta H = \Delta E + \delta E_{Solv} + \delta E_{DFTD3BJ} + \delta E_H \qquad (3)$$

where ΔE, and δE_{Solv} are computed at the B3PW91/ECP2 level, δE_G and δE_H are computed at the RI- B3PW91/ECP1 level. WBIs were computed during natural population analysis.[69] The energy spans and free energies for the product dissociation were obtained after counterpoise corrections, which were calculated by performing single-point calculations at the B3PW91/ECP2 level (see Tables S5a – S5p on the SI). All calculations were performed using Gaussian 09.[70]

Conflicts of interest

There are no conflicts to declare.

Acknowledgements

Notes and references

1. B. Cornils, W. A. Herrmann, M. Beller, R. Paciello, *Applied Homogeneous Catalysis with Organometallic Compounds*: A Comprehensive Handbook in Four Volumes, Wiley-VCH Verlag GmbH Co. KGaA, Germany, 2003.
2. M. Beller, Editor, C*atalytic Carbonylation Reactions.* [Inn: Top. Organomet. Chem.; 2006, 18], Springer GmbH, 2006.
3. L. Kollar, Editor, *Modern Carbonylation Methods*, Wiley-VCH Verlag GmbH Co. KGaA, 2008.
4. S. S. Stahl, *J. Am. Chem. Soc.*, 2010, **132**, 8524-8525.

ARTICLE

Journal Name

5. X.-F. Wu, H. Neumann and M. Beller, *Chem. Rev. (Washington, DC, U. S.)*, 2013, **113**, 1-35.
6. X.-F. Wu, H. Neumann and M. Beller, *Chem. Soc. Rev.*, 2011, **40**, 4986-5009.
7. E. Drent, P. Arnoldy and P. H. M. Budzelaar, *J. Organomet. Chem.*, 1993, **455**, 247-253.
8. E. Drent, P. Arnoldy and P. H. M. Budzelaar, *J. Organomet. Chem.*, 1994, **475**, 57-63.
9. A. Dervis, P. G. Edwards, P. D. Newman, R. P. Tooze, S. J. Colesa and M. B. Hursthouse, *J. Chem. Soc., Dalton Trans.*, 1999, 1113-1119.
10. A. Dervisi, P. G. Edwards, P. D. Newman and R. P. Tooze, *Dalton*, 2000, 523-528.
11. A. Scrivanti, V. Beghetto, E. Campagna, M. Zanato and U. Matteoli, *Organometallics*, 1998, **17**, 630-635.
12. A. Scrivanti, M. Bertoldini, V. Beghetto, U. Matteoli and A. Venzo, *J. Organomet. Chem.*, 2008, **694**, 131-136.
13. C. S. Consorti, G. Ebeling and J. Dupont, *Tetrahedron Lett.*, 2002, **43**, 753-755.
14. G. Kiss, *Chem. Rev. (Washington, D. C.)*, 2001, **101**, 3435-3456.
15. Shell (E. Drent, D. H. L. Pello), Patent no. WO 95/03269A1, 1995.
16. Shell (P. Arnoldy, A. P. M. Kremers), Patent no. EP 56/5199A2, 1993.
17. F. Niele, *Chem. Mag. (Rijswijk, Neth.)*, 1995, 12.
18. J. Keijsper, P. Arnoldy, M. J. Doyle and E. Drent, *Recl. Trav. Chim. Pays-Bas*, 1996, **115**, 248-255.
19. J. Andrieu, B. R. Steele, C. G. Screttas, C. J. Cardin and J. Fornies, *Organometallics*, 1998, **17**, 839-845.
20. B. A. Trofimov, R. N. Kudyakova, A. G. Mal'kina, V. V. Nosyreva, N. A. Kalinina and A. I. Albanov, *Dokl. Akad. Nauk*, 2001, **378**, 61-63.
21. A. G. Mal'kina, R. N. Kudyakova, V. V. Nosyreva, A. V. Afonin and B. A. Trofimov, *Russ. J. Org. Chem.*, 2002, **38**, 1088-1092.
22. B. Harris, *Ingenia*, 2010, 18–23.
23. M. Moukwa, *Journal*, 2010, 50–52.
24. W. Clegg, G. R. Eastham, M. R. J. Elsegood, B. T. Heaton, J. A. Iggo, R. P. Tooze, R. Whyman and S. Zacchini, *Organometallics*, 2002, **21**, 1832-1840.
25. W. Clegg, M. R. J. Elsegood, G. R. Eastham, R. P. Tooze, X. L. Wang and K. Whiston, *Chem. Commun. (Cambridge)*, 1999, DOI: 10.1039/a905521e, 1877-1878.
26. G. R. Eastham, R. P. Tooze, M. Kilner, D. F. Foster and D. J. Cole-Hamilton, *J. Chem. Soc., Dalton Trans.*, 2002, DOI: 10.1039/b201514e, 1613-1617.
27. E. Zuidema, C. Bo and P. W. N. M. Van Leeuwen, *J. Am. Chem. Soc.*, 2007, **129**, 3989-4000.
28. A. Dervisi, P. G. Edwards, P. D. Newman, R. P. Tooze, S. J. Coles and M. B. Hursthouse, *J. Chem. Soc., Dalton Trans.*, 1998, 3771-3776.
29. L. Crawford, D. J. Cole-Hamilton, E. Drent and M. Bühl, *Chem. - Eur. J.*, 2014, **20**, 13923-13926.
30. L. Crawford, D. J. Cole-Hamilton and M. Bühl, *Organometallics*, 2015, **34**, 438-449.
31. F. Y. Petillon, J. L. Le Quere, F. Le Floch-Perennou, J. E. Guerchais, M. B. Gomes de Lima, L. J. Manojlovic-Muir, K. W. Muir and D. W. A. Sharp, *J. Organomet. Chem.*, 1983, **255**, 231-244.
32. B. Fell, H. U. Hoeg and C. Krueger, *J. Mol. Catal.*, 1985, **30**, 57-71.
33. H. L. Stokes, T. L. Smalley, Jr., M. L. Hunter, M. E. Welker and A. L. Rheingold, *Inorg. Chim. Acta*, 1994, **220**, 305-318.
34. H. Adams, N. A. Bailey, J. T. Gauntlett, I. M. Harkin, M. J. Winter and S. Woodward, *J. Chem. Soc., Dalton Trans.*, 1991, 1117-1128.
35. M. H. Cheng, G. H. Lee, S. M. Peng and R. S. Liu, *Organometallics*, 1991, **10**, 3600-3606.
36. T.-a. Mitsudo, K.-i. Fujita, S. Nagano, T.-a. Suzuki, Y. Watanabe and H. Masuda, *Organometallics*, 1995, **14**, 4228-4235.
37. K. B. Wiberg, *Tetrahedron*, 1968, **24**, 1083-1096.
38. S. Kozuch and S. Shaik, *J. Am. Chem. Soc.*, 2006, **128**, 3355-3365.
39. S. Kozuch, S. E. Lee and S. Shaik, *Organometallics*, 2009, **28**, 1303-1308.
40. S. Kozuch and S. Shaik, *Acc. Chem. Res.*, 2011, **44**, 101-110.
41. We do not wish to overinterpret DFT computed energy differences of less than 1 kcal mol^{-1}, but note that the computed trends are qualitatively consistent with the observations.
42. Shell (E. Drent, W. W. Jager, J. C. L. J. Suykerbuyk), Patent no. WO 95/05357, 1995.
43. A. B. Pangborn, M. A. Giardello, R. H. Grubbs, R. K. Rosen and F. J. Timmers, *Organometallics*, 1996, **15**, 1518-1520.
44. H. Schmidbaur and Y. Inoguchi, *Z. Naturforsch., B: Anorg. Chem., Org. Chem.*, 1980, **35B**, 1329-1334.
45. D. Cuperly, P. Gros and Y. Fort, *J. Org. Chem.*, 2002, **67**, 238-241.
46. T. Zhang, Y. Qin, D. Wu, R. Zhou, X. Yi and C. Liu, *Synth. Commun.*, 2005, **35**, 1889-1895.
47. L. Hintermann, T. T. Dang, A. Labonne, T. Kribber, L. Xiao and P. Naumov, *Chemistry*, 2009, **15**, 7167-7179.
48. M. L. Clarke, D. J. Cole-Hamilton, D. F. Foster, A. M. Z. Slawin and J. D. Woollins, *J. Chem. Soc., Dalton Trans.*, 2002, DOI: 10.1039/b200401a, 1618-1624.
49. A. D. Becke, *J. Chem. Phys.*, 1996, **54**, 1040-1046.
50. J. P. Perdew, K. Burke and Y. Wang, *Phys. Rev. B: Condens. Matter*, 1996, **54**, 16533-16539.
51. J. P. Perdew, J. A. Chevary, S. H. Vosko, K. A. Jackson, M. R. Pederson, D. J. Singh and C. Fiolhais, *Phys. Rev. B: Condens. Matter*, 1992, **46**, 6671-6687.
52. L. Wang, Y. Zhang, H. He and J. Zhang, *Synth. Met.*, 2013, **167**, 51-63.
53. P. L. Arnold, E. Hollis, G. S. Nichol, J. B. Love, J.-C. Griveau, R. Caciuffo, N. Magnani, L. Maron, L. Castro, A. Yahia, S. O. Odoh and G. Schreckenbach, *J. Am. Chem. Soc.*, 2013, **135**, 3841-3854.
54. S. Salman, J.-L. Bredas, S. R. Marder, V. Coropceanu and S. Barlow, *Organometallics*, 2013, **32**, 6061-6068.
55. M. M. Montero-Campillo, A. M. Lamsabhi, O. Mo and M. Yanez, *Theor. Chem. Acc.*, 2013, **132**, 1-8.
56. S. K. Ignatov, S. V. Panteleev, S. V. Maslennikov and I. V. Spirina, *Russ. J. Gen. Chem.*, 2012, **82**, 1954-1961.
57. S. Grimme, J. Antony, S. Ehrlich and H. Krieg, *J. Chem. Phys.*, 2010, **132**, 154104/154101-154104/154119.
58. S. Grimme, S. Ehrlich and L. Goerigk, *J. Comput. Chem.*, 2011, **32**, 1456-1465.
59. T. Risthaus and S. Grimme, *J. Chem. Theory Comput.*, 2013, **9**, 1580-1591.

60. A. D. Becke and E. R. Johnson, *J. Chem. Phys.*, 2007, **127**, 154108/154101-154108/154106.

61. E. R. Johnson and A. D. Becke, *J. Chem. Phys.*, 2006, **124**, 174104/174101-174104/174109.

62. M. K. Kesharwani and J. M. L. Martin, *Theor. Chem. Acc.*, 2014, **133**, 1-14.

63. C. Peng, P. Ayala, H. B. Schlegel and M. J. Frisch, *J. Comput. Chem.*, 1996, **17**, 49-56.

64. C. Gonzalez and H. B. Schlegel, *J. Chem. Phys.*, 1989, **90**, 2154-2161.

65. C. Gonzalez and H. B. Schlegel, *J. Phys. Chem.*, 1990, **94**, 5523-5527.

66. J. Tomasi, B. Mennucci and E. Cances, *J. Mol. Struct.: THEOCHEM*, 1999, **464**, 211-226.

67. J. Tomasi, B. Mennucci and R. Cammi, *Chem. Rev. (Washington, DC, U. S.)*, 2005, **105**, 2999-3093.

68. A. Klamt, B. Mennucci, J. Tomasi, V. Barone, C. Curutchet, M. Orozco and F. J. Luque, *Acc. Chem. Res.*, 2009, **42**, 489-492.

69. A. E. Reed, L. A. Curtiss and F. Weinhold, *Chem. Rev.*, 1988, **88**, 899-926.

70. M. J. T. Frisch, G. W.; Schlegel, H. B.; Scuseria, G. E.; Robb, M. A.; Cheeseman, J. R.; Scalmani, G.; Barone, V.; Mennucci, B.; Petersson, G. A.; Nakatsuji, H.; Caricato, M.; Li, X.; Hratchian, H. P.; Izmaylov, A. F.; Bloino, J.; Zheng, G.; Sonnenberg, J. L.; Hada, M.; Ehara, M.; Toyota, K.; Fukuda, R.; Hasegawa, J.; Ishida, M.; Nakajima, T.; Honda, Y.; Kitao, O.; Nakai, H.; Vreven, T.; Montgomery, J. A., Jr.; Peralta, J. E.; Ogliaro, F.; Bearpark, M.; Heyd, J. J.; Brothers, E.; Kudin, K. N.; Staroverov, V. N.; Kobayashi, R.; Normand, J.; Raghavachari, K.; Rendell, A.; Burant, J. C.; Iyengar, S. S.; Tomasi, J.; Cossi, M.; Rega, N.; Millam, J. M.; Klene, M.; Knox, J. E.; Cross, J. B.; Bakken, V.; Adamo, C.; Jaramillo, J.; Gomperts, R.; Stratmann, R. E.; Yazyev, O.; Austin, A. J.; Cammi, R.; Pomelli, C.; Ochterski, J. W.; Martin, R. L.; Morokuma, K.; Zakrzewski, V. G.; Voth, G. A.; Salvador, P.; Dannenberg, J. J.; Dapprich, S.; Daniels, A. D.; Farkas, Ö.; Foresman, J. B.; Ortiz, J. V.; Cioslowski, J.; Fox, D. J., *Journal*, 2009.

71. S. Ahmad, A. Lockett, T. A. Shuttleworth, A. Miles-Hobbs, P. G. Pringle, M. Bühl, Palladium–catalysed Alkyne Alkoxycarbonylation with P,N Chelating Ligands Revisited: A Density Functional Theory Study (Dataset), University of St Andrews Research Portal. 2019. https://doi.org/XXXX